Wear 532-533 (2023) 205095

Contents lists available at ScienceDirect

Wear

journal homepage: www.elsevier.com/locate/wear

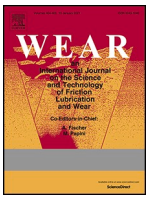

Investigating the self-lubricating properties of novel TiSiVN coating during dry turning of Ti6Al4V alloy

Ch Sateesh Kumar [a,b,*], Gorka Urbikain [a,b], Pablo Fernández De Lucio [a,b], Luis Norberto López De Lacalle [a,b], Cristian Pérez-Salinas [a,b], Soumya Gangopadhyay [c], Filipe Fernandes [d,e]

[a] CFAA- Aeronautics Advanced Manufacturing Center, University of the Basque Country (UPV/EHU), Biscay Science and Technology Park, Ed. 202, Zamudio, Spain
[b] Department of Mechanical Engineering, University of the Basque Country, Escuela Superior de Ingenieros Alameda de Urquijo S/N, 48013, Bilbao, Spain
[c] Department of Mechanical Engineering, Indian Institute of Technology Bhilai, Raipur, 492015, Chhattisgarh, India
[d] University of Coimbra, CEMMPRE, ARISE, Department of Mechanical Engineering, Rua Luís Reis Santos, 3030-788, Coimbra, Portugal
[e] ISEP, Polytechnic of Porto, Rua Dr. António Bernardino de Almeida, 4249-015, Porto, Portugal

ARTICLE INFO

Keywords:
TiSiVN
Self-lubricating coatings
Tool wear
Ti6Al4V alloy
Machining

ABSTRACT

The machining of titanium alloys like Ti6Al4V has been challenging owing to their low thermal conductivity, making them highly difficult-to-cut. Many techniques have been adopted to improve machinability of Ti6Al4V titanium alloy and the durability of the cutting tools during its machining. Thus, to improve their machinability, the current work investigates the applicability of TiSiVN self-lubricating coating deposited on Al_2O_3–SiC ceramic cutting tools during continuous turning of Ti6Al4V alloy under dry cutting environment. The TiSiVN coating accounted for lower surface roughness and cutting temperatures under all conditions. Due to the formation of V_2O_5 at high temperatures that were observed during oxidation and machining tests in EDS and Raman spectroscopy, the TiSiVN coating helped in reducing friction and, thus, retained the crater wear area. In contrast, the worn area on the crater surface reduced for uncoated and TiSiN coated cutting tools due to a significant increase in nose depth decrement with increasing cutting speed. Furthermore, increased nose depth decrement resulted in the drop of machining forces when using TiSiN coated and uncoated cutting tools. However, the coating delamination due to oxidation was apparent which reduced the effectiveness of lubricious phases present in the cutting zone for TiSiVN coated tool.

1. Introduction

The favorable mechanical properties such as wear resistance, high strength-to-weight ratio, corrosion resistance, and biocompatibility of titanium alloys make them an excellent choice as a material for demanding applications not only in the aerospace industry but also in gas and oil, and bio-medical industries [1,2]. However, the lower elastic modulus and thermal conductivity, high chemical reactivity, and hardening due to plastic deformation and diffusion act as significant disadvantages during machining of titanium alloys categorizing them as highly difficult-to-cut materials [1,3,4]. These disadvantages lead to application of lower cutting speeds during machining of titanium and its alloys.

A possible solution to improve the machinability and cutting tool durability is to reduce friction at the tool-chip interface, causing decrease in the amount of heat trapped at the cutting zone that occurred due to the lower thermal conductivity of titanium alloys. Reducing friction would help decrease cutting temperatures for any machining operation and, thus, enhance the cutting tool's durability [5–7]. Many researchers have tested the possibility of different thin-film systems on cutting tools during machining of titanium alloys for improving their machinability and cutting tool durability. In this regard, Sui et al. [8] reported that the TiSiAlN coating, due to its high hardness and superior wear resistance, improved cutting tool durability substantially during machining Ti6Al4V alloy. These conventional coatings, like TiAlN, TiSiN, AlTiN etc., provide superior wear and oxidation resistance over the substrate [9–12]. Also, these coatings exhibit a lower apparent coefficient of friction due to their anti-adhesive properties [13–15].

* Corresponding author. CFAA- Aeronautics Advanced Manufacturing Center, University of the Basque Country (UPV/EHU), Biscay Science and Technology Park, Ed. 202, Zamudio, Spain.
E-mail address: chigullasateesh.kumar@ehu.eus (C.S. Kumar).

https://doi.org/10.1016/j.wear.2023.205095
Received 6 July 2023; Accepted 13 August 2023
Available online 14 August 2023

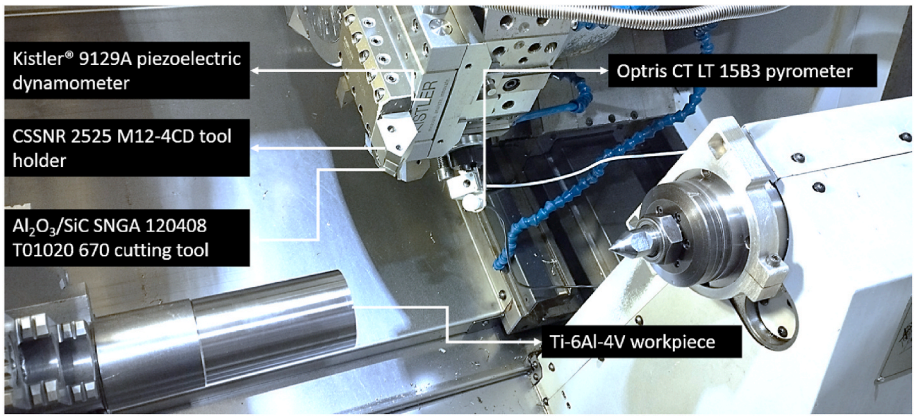

Fig. 1. Experimental Setup for dry turning of Ti6Al4V workpiece.

Table 1
Morphology (surface and cross-sectional), chemical composition, and mechanical properties of the produced coatings.

Sample/Coating	TiSiN	TiSiVN
Cross-sectional morphology	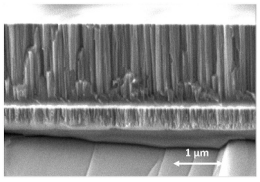	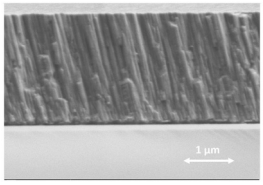
Surface morphology	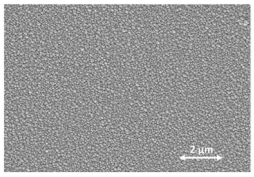	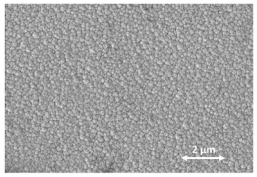
chemical composition (at. %)	Ti – 31.9 ± 0.3 Si – 14.9 ± 0.2 N – 53.3 ± 0.4 Ar – 0.3 ± 0.11	Ti – 24.9 ± 0.3 Si – 11.6 ± 0.2 N – 55.1 ± 0.45 Ar – 0.2 ± 0.12 V – 7.2 ± 0.13
Hardness (GPa)	21 ± 2	20 ± 2
Elastic modulus (GPa)	242 ± 9	234 ± 13
Adhesion critical loads (N)	Lc1 = 43 ± 2 Lc2 = 50 ± 3 Lc3 = 62 ± 3	Lc1 = 45 ± 3 Lc2 – 61 ± 2 Lc3 – NA
Surface roughness (μm)	0.534 ± 0.021	0.523 ± 0.025

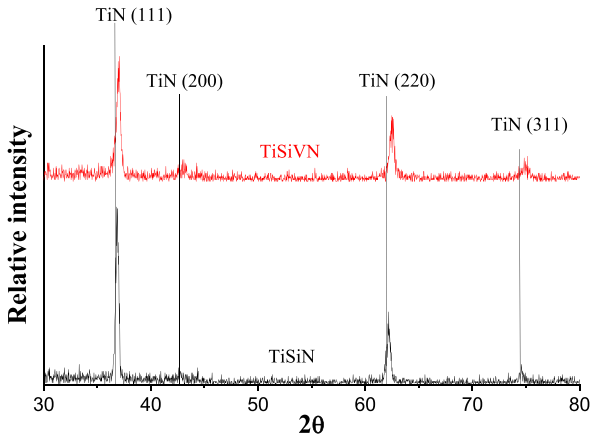

Fig. 2. XRD diffraction patterns of the as-deposited coatings.

However, there are no means of generating lubrication at the tool-chip interface, which is an essential solution for the machinability improvement of titanium alloys. However, the self-lubricating coatings that provide superior wear and oxidation resistance due to the generation of lubricious phases at elevated temperatures could be helpful [16]. Due to their crystallographic planes with reduced binding energy, the Magnéli oxide phases of Ti, W, V, or Mo act as a solid lubricating agent and, thus, reduce friction [17]. Mainly, V addition to transition metal nitrides at elevated temperatures accounts to rapid oxidation of coatings (e.g., AlCrSiVN, TiSiVN) causing formation of V_nO_{3n-1} low melting point lubricious phases. These phases results in the reduction of coefficient of friction [18]. These coatings are applied in various high-temperature processes involving sliding surfaces like machining [19]. TiSiVN coating is of enhanced interest due to its ability to form a rapid tribo-layer on the surface that could reduce friction [20]. However, not much literature is available that studies the performance of self-lubricating coatings with V for machining of titanium alloys.

Further, the literature lacks in investigations on oxidation and diffusion taking place during the machining of titanium alloys while machining with coated self-lubricating cutting tools. Apart from

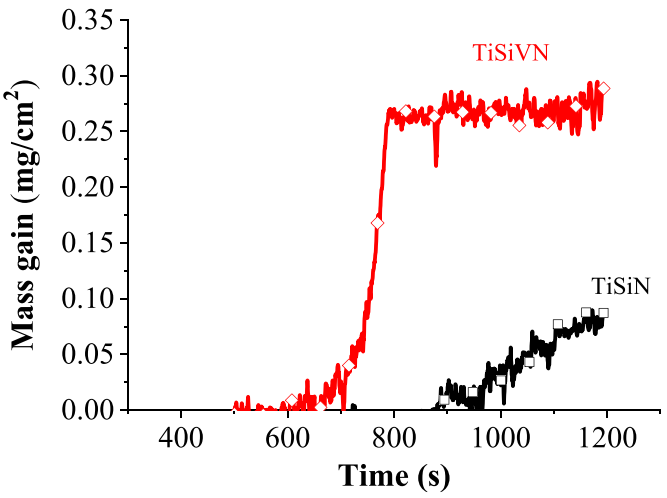

Fig. 3. Thermogravimetric curves of coatings using the linear-temperature ramp from RT to 1200 °C at 20 °C/min).

coatings, another possible solution for higher cutting tool durability can be cutting tools with high operating temperatures that can withstand thermal shocks for prolonged periods. The Al_2O_3-based ceramic tools with reinforcements like TiCN, TiC, SiC whiskers, etc., effectively improve the thermal shock resistance and fracture toughness of the Al_2O_3 ceramic matrix [21], which is highly brittle with low tensile strength [15]. Also, forces play a significant role in defining the machining performance of cutting tools. Moreover, the coatings can impact the machining forces by lowering friction and tool wear due to superior wear resistance, self-lubrication, and reduced heat transmission [22–24]. Further, the fluctuation in forces can significantly impact chipping and elevating tool wear in cutting tools [25]. Thus, the present work aims to investigate the influence of TiSiVN self-lubricating coating on machining forces, wear behavior and rake-surface topography of Al_2O_3 cutting tool with SiC whiskers reinforcement during turning of Ti6Al4V titanium alloy under dry cutting environment.

2. Experimental methodology

2.1. Coating deposition and characterization

Using DC power sources and a 4-target semi-industrial type PVD TEER sputtering equipment, thin films of TiSiN and TiSiVN were deposited. Four cathodes are uniformly spaced across the chamber with respect to its center. For the depositions, high-purity Ti, Si, and V targets were employed. Ti targets were placed in cathodes 1 and 3, facing each other, and V and Si targets were placed in cathodes 2 and 4, making 90° with the other targets. For optimal performance, applying coatings onto a well-prepared substrate is essential.

Additionally, applying certain post-treatments can further enhance the performance of the coating [26] because at high speeds [27] or high feed values [28], pre and post-treatments are vital in preserving the coating layer integrity. The chamber was evacuated to 7.5×10^{-6} mbar of pressure prior to the depositions. A pulsed bias of 650 V and a frequency of 250 kHz were used to etch the substrates for the first 40 min in an Ar environment. The two Ti targets were cleaned for 20 min with 1000 W applied to each of them throughout the etching process. The Si target then received 300 W for another 20 min, and the V target received 1000 W. To prevent cross-contamination between the targets and the substrate during the etching step of the process, a pair of shutters were placed in front of each pair of targets.

After the etching process, a Ti adhesion layer was deposited over the substrate, lasting 10 min, while applying 2500 W to each Ti target. Then, a gradient layer of TiN with increasing nitrogen content each minute, up to 12 sccm, was deposited for 10 min. Then the final films were deposited. The TiSiN film was produced by applying 2500 W to each Ti target and 1200 W to the Si target, using 20 sccm of Ar and 17 sccm of N_2 for 240 min. The deposition pressure was 2.7×10^{-3} mbar.

On the other hand, the TiSiVN films as produced using the same parameters used for the TiSiN film, with the additional power applied to the V target of 100W. The deposition pressure was 3.1×10^{-3} mbar. All the depositions were performed with the substrate holder rotating to 23 rpm, applying a pulsed bias of −50V and a deposition time of 240 min. The coatings were deposited onto i) silicon wafers (111) for chemical, cross-sectional and surface morphology analysis, structural analysis, and mechanical properties evaluation (hardness and Young's modulus) and ii) alumina substrates for oxidation tests and iii) Al_2O_3–SiC whisker reinforced ceramic inserts for scratch and machining tests. The chemical composition of the coatings was acquired by wavelength dispersive spectrometer (WDS) from Bruker (Model: QUANTAX WDS). Standard specimens were used to calibrate the signal of the different elements. The cross-section and surface morphology of the coatings was observed using scanning electron microscope (SEM) from ZEISS (Model: Merlin®). The crystallographic structure of the coatings was investigated with X-Ray Diffraction (XRD) with the help of X' PertPro MPD diffractometer using copper Kα1 radiation (λ = 1.54) in grazing incident mode. The hardness and Young's modulus of the coatings was evaluated

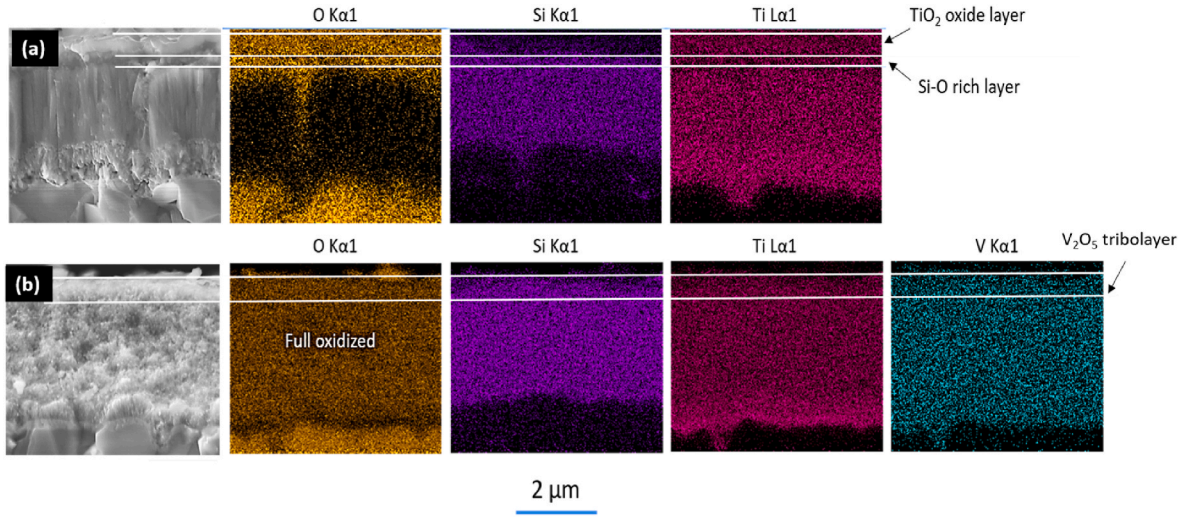

Fig. 4. Cross section morphology of oxidized films and corresponding elemental maps distribution-a) TiSiN and b) TiSiVN.

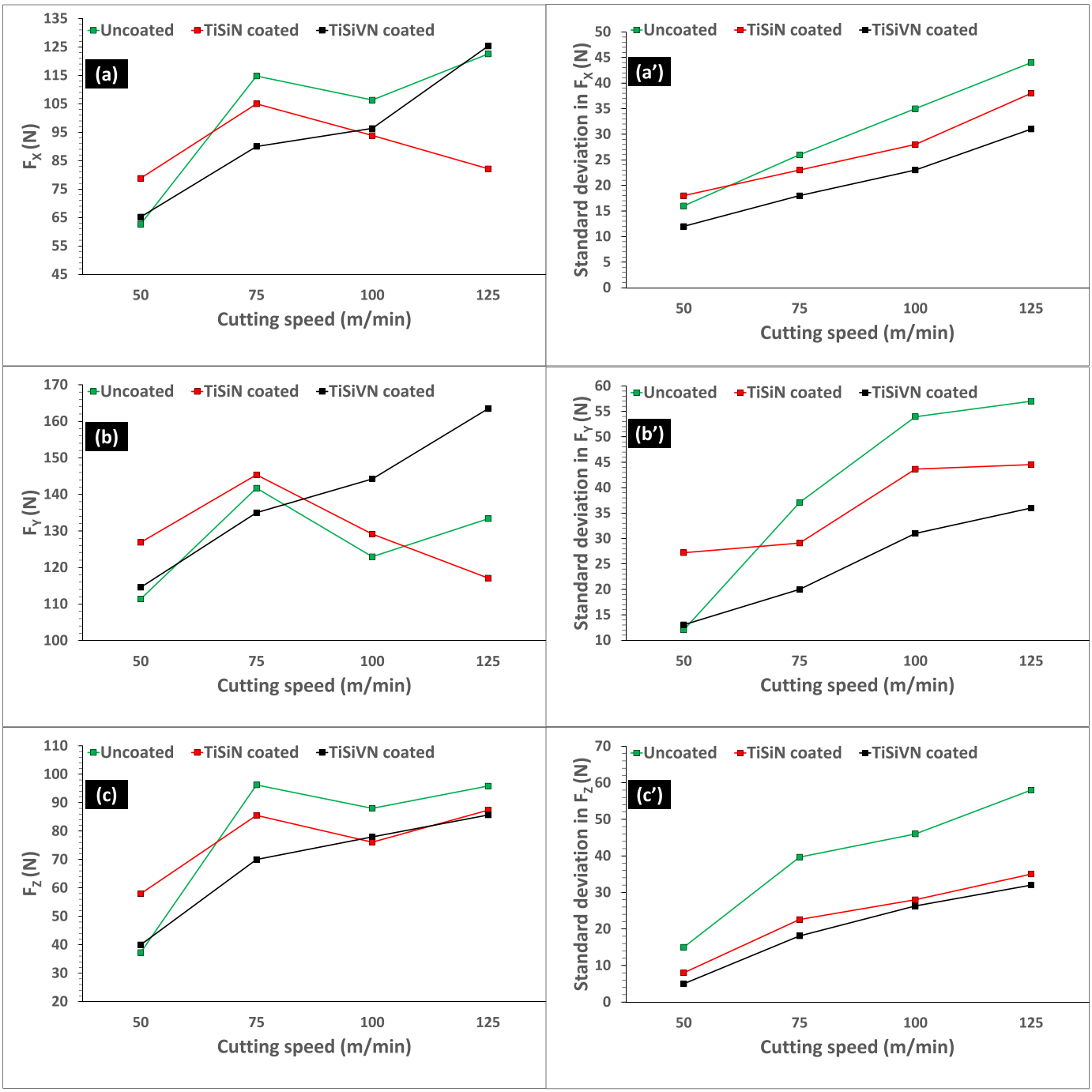

Fig. 5. Variation of averaged measured forces (a, b, and c) and standard deviation of forces (a', b', and c') with cutting speed.

by nanoindentation. The tests were conducted using a Berkovich diamond pyramid indenter. The indentation depth was kept less than 10% of the coating thickness to avoid the contribution of the substrate. A scratch-tester was used to assess the adhesion of the films to the Al_2O_3–SiC substrates.

Utilizing a Rockwell C indenter with a spherical tip having radius of 0.2 mm, a scratch speed of 10 mm/min, and a loading speed of 100 N/min, specimens were scratched while the normal force was ramped linearly from 5 to 70 N. An optical microscope was used to determine the critical loads. The beginning point of the oxidation of the films was identified using the thermogravimetric analysis (TGA). TGA study was performed in industrial air (99.99% pure) with a continuous temperature rise from room temperature (RT) up to 1200 °C at 20 °C/min in order to better understand the oxidation behavior of TiSiN and TiSiVN coatings. The oxidation weight increase brought on by oxygen entrance was continuously tracked while the films were exposed to a linear temperature ramp that was constant throughout. The cross-sectional morphology of the oxidized coated samples was examined using SEM to evaluate the size of the oxidation zone.

2.2. *Machining tests and measurements*

A CMZ TC25BTY turning center with an integrated spindle and 35 kW of spindle power was used for the tests. A triaxial Kistler® 9129A

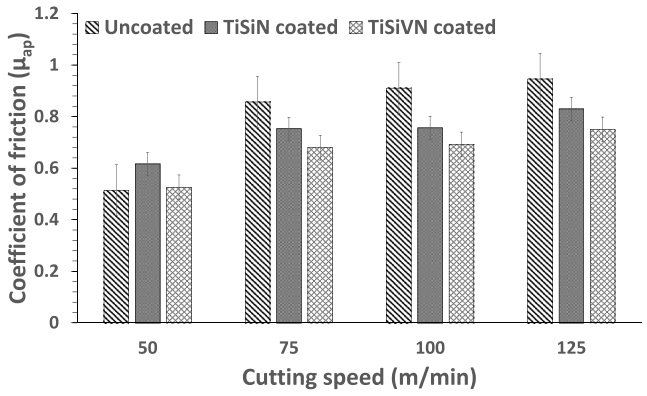

Fig. 6. Coefficient of friction variation with cutting speed.

piezoelectric dynamometer and an OROS® OR35 real-time multi-analyzer with a sampling frequency of 12,800 samples/s were used to measure cutting forces. The data points obtained by the dynamometer as a function of time are then averaged to determine the average machining forces. Further, a standard deviation in the machining forces is obtained using Equation (1) which takes into consideration the force value at each data point.

$$\sigma_{std} = \frac{\sqrt{\sum (F - F_{avg})^2}}{N} \quad (1)$$

Where σ_{std} is the standard deviation, F is the value of force at a given time, and F_{avg} is the average value of the force, and N is the number of data points.

The experimental setup for the testing is shown in Fig. 1. All cutting tests were performed using SNGN 120408 T01020 670 Al_2O_3–SiC whiskers reinforced cutting tools (70% Al_2O_3 and 30% SiC) with and without coating depositions placed on a CSSNR 2525 M12-4CD tool holder. For each coating under evaluation, a total of four cutting speeds (50, 75, 100, and 125 m/min) were employed. The ceramic tools had a measured hardness of 25.3 ± 0.2 GPa and surface roughness of 0.488 ± 0.031 μm, whereas the fracture toughness was around 4.5 ± 0.3 $MPam^{1/2}$ [21].

At 0.1 mm/rev and 0.5 mm, respectively, the feed rate and depth of cut remained unchanged. Having a diameter of 100 mm and a length of 250 mm, the Ti6Al4V alloy workpiece used was an aged round bar with hardness of 35 ± 2 HRC. 100 mm of cut length, however, was employed for the cutting tests. To determine the impact of coatings, tests were conducted in dry circumstances. For the purpose of preventing machining errors due to vibrations, tool and workpiece mounting, and chip winding, each test was conducted three times, and the mean value of all the forces, temperatures, and surface roughness were determined for comparison. Using a Taylor Hobson Surtronic Duo 03M980 surface roughness tester, the surface roughness, or R_A, was measured. For each replicate of the experiment, readings were obtained on three separate places of the workpiece, and they were then averaged. An Optris CT LT 15B3 non-contact pyrometer installed on the machine tool was used to monitor the temperature. The sensor was pointed to the cutting zone to record accurate cutting temperatures during machining. An average recorded temperature over the cut length was considered the cutting temperature (CT). The apparent coefficient of friction (μ_{ap}) was calculated based on the below equation [14].

$$\mu_{ap} = \frac{F_{XZ} + F_Y \tan\propto}{F_Y - F_{XZ} \tan\propto} \quad (2)$$

$$F_{XZ} = \sqrt{F_X{}^2 + F_Y{}^2} \quad (3)$$

Where F_Y is the cutting force, F_X is the feed force, F_Z is the thrust force, F_{XZ} is the equivalent thrust force and ∝ is the orthogonal rake angle (-8°). SEM with EDS was used to study the wear mechanisms on the cutting tools. The topography measurements for crater depth, crater volume and crater area were made using Sensoview 1.6.0 software. The topography results were validated by comparing them with measurements made on SEM and optical microscope. Etching with acetone was carried out before making all the topography measurements.

3. Results and discussion

3.1. Coating characterization

The surface and cross-section morphologies, mechanical characteristics, adhesion critical loads, and chemical composition of the as-deposited coatings are all summarized in Table 1. The cross-sectional morphology of both TiSiN and TiSiVN coatings was columnar with coating thickness of approximately 2.21 and 2.25 μm, respectively. V additions produce a more columnar cross-section morphology, which agrees with the larger features in the film's top surface corresponding to the end of the columns [20]. Both films displayed an over-stoichiometric composition, with the N concentration slightly higher than the sum of the metallic elements presented on the coatings (Ti, Si, and V). As expected, the power set at the V target allowed the production of a coating with V additions. Although adding V reduced the Ti and Si concentrations on the coating, the ratio between Ti/Si remained constant, clearly revealing that both films have similar Ti and Si concentrations in proportion. Both the films displayed considerable adhesion to the substrate

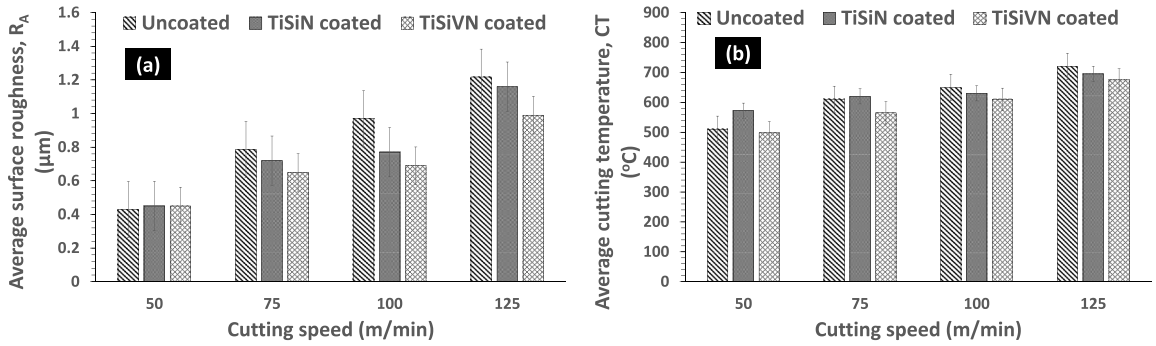

Fig. 7. (a) Average surface roughness (R_A) and (b) average cutting temperature (CT) variation with cutting speed.

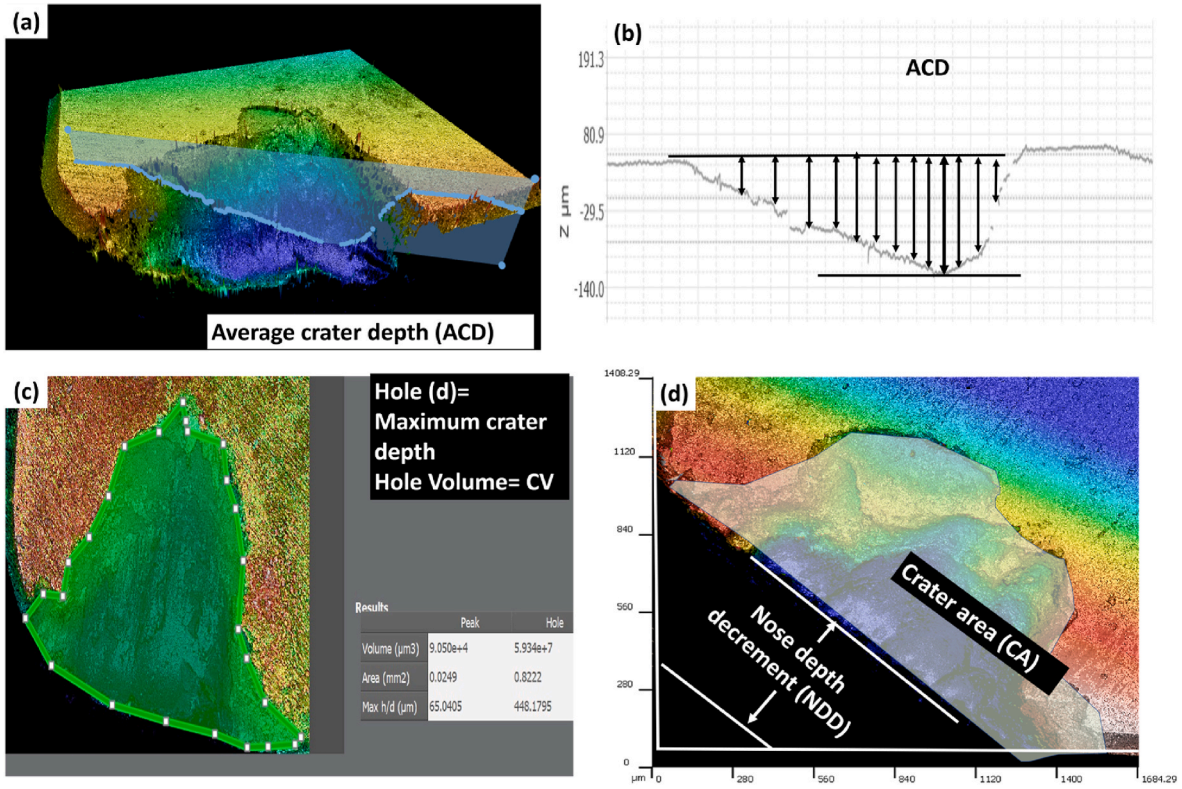

Fig. 8. Representative measurement of (a and b) average crater depth (ACD), (b) crater volume (CV) (d) nose depth decrement (NDD) and crater area (CA).

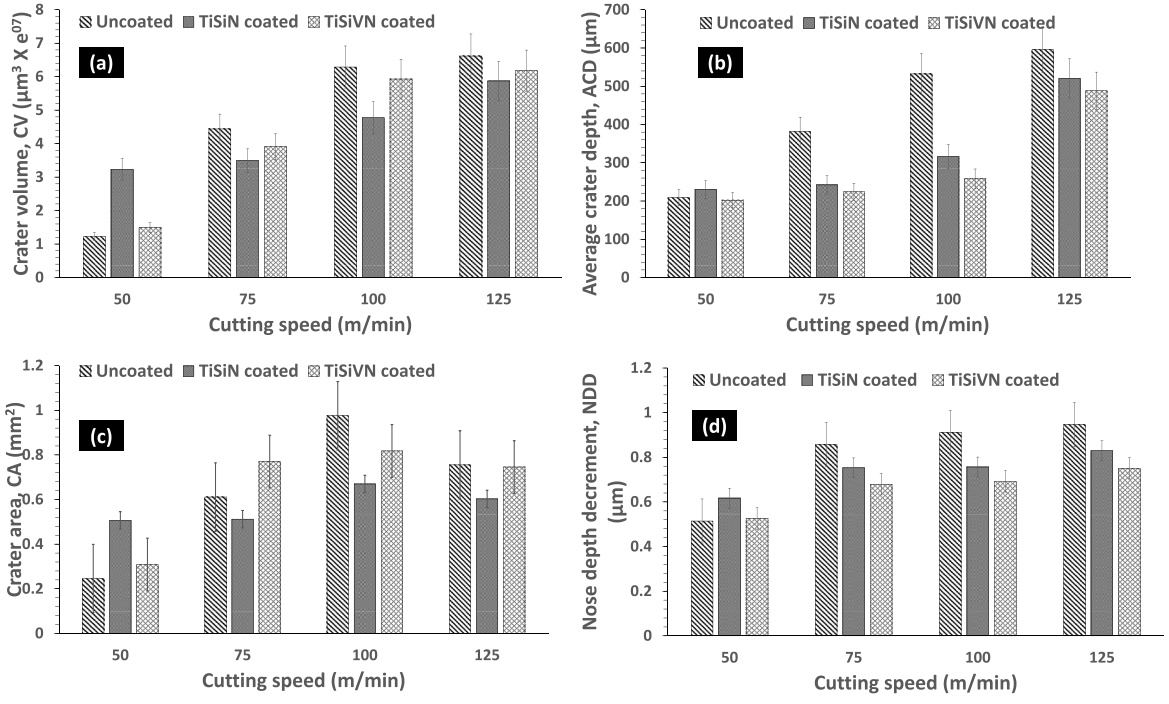

Fig. 9. (a) Crater volume (CV), average crater depth (ACD), crater area (CA), and nose depth decrement (NDD) plotted against cutting speed.

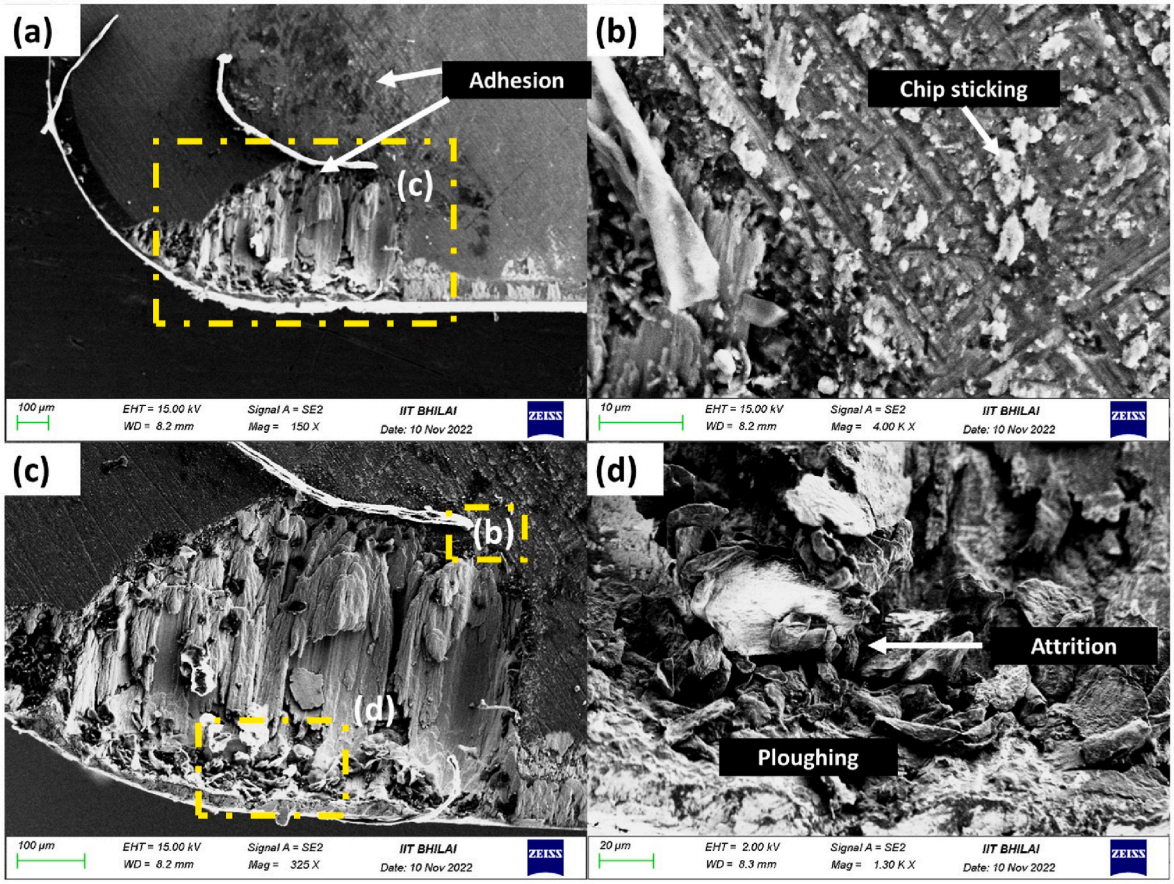

Fig. 10. SEM micrographs of the rake face of the uncoated Al_2O_3–SiC whiskers reinforced cutting after machining Ti6Al4V alloy at 50 m/min cutting speed.

with the first coating cracking occurring in the range of 41–48 N. The first coating chipping occurs for 50 and 61 N for TiSiN and TiSiVN coatings, respectively. Full substrate exposure occurs for TiSiN coating at 62 N, while up to 70 N, no Lc3 adhesion failure was detected for TiSiVN coating. V additions, as shown in Table 1, do not significantly change the hardness and Elastic modulus values of the coatings.

The XRD diffraction patterns of the coatings are presented in Fig. 2. As expected, both coatings display diffraction peaks with NaCl-type structure assigned to crystalline TiN (f.c.c. NaCl type TiN phase ICDD card no. 01-087-0633) with Si and V in solid solution [29], which is in good agreement with the authors' previous works. Nonetheless, it should be noted that since the Si concentration on the coatings is higher than 4 at.%, Si–N phase should also be present in the structure; however, due to their amorphous character, it is not detected by XRD [30].

The mass gain with time during TGA tests has been plotted in Fig. 3. The reference TiSiN film begins to oxidize roughly at 900 °C which is comparable to that reported by Fernandes et al. [31] for coatings with similar chemical composition. A similar oxidation temperature was reported by Mortiz et al. [32] for arc evaporation deposited TiSiN coatings. Later, the weight gain increases slowly, reaching a value of 0.10 mg/cm^2 at 1200 °C. According to the coating's cross-section morphology, a very small oxidized zone can be noticed (see Fig. 4). The oxide scale was composed of a Ti–O layer on top and a Si–O-rich layer below as confirmed by the EDS elemental maps presented in the same figure. The coating rich in V displayed a much lower onset point of oxidation, i.e., the coating starts to oxidize at 600 °C. The temperature increase to ~800 °C, led to a sharp rise of the mass gain due to the oxidation. At this temperature, the curve displayed a plateau, suggesting a complete oxidation of the film, as confirmed by the O elemental maps of the oxidized cross-section. The lower and fast oxidation resistance of V-rich coatings has been attributed to the fast diffusion of V to the surface of the coatings, which disrupted the formation of protective oxide scales, as is the case of Si–O formed in the TiSiN coating [20]. The diffusion of V to the surface has been reported to form different V–O compounds, mainly the V_2O_5 phase, which in the contacts has been responsible for providing low friction properties [33].

3.2. Forces and friction

The standard deviation of observed average forces and their fluctuation with cutting speed are shown in Fig. 5. For a tool coated with TiSiVN, the machining forces rise with cutting speed; whereas, for an uncoated tool, the machining forces increase at first and subsequently decrease as cutting speed increases. With increasing cutting speeds, the standard deviation in machining forces rises, which might severely affect tool life and the quality of the machined surface. The higher standard deviation in machining forces may lead to higher stress fluctuations on the tool leading to chatter causing damage initiation [25]. When compared to uncoated and TiSiN-coated cutting tools, the TiSiVN-coated tool always has a lower standard deviation in forces. Additionally, it is intriguing to note that the forces for coated tools, particularly those with a TiSiVN self-lubricating coating, correspond to greater averaged machining forces with a smaller standard deviation, indicating lesser machining vibrations when using TiSiVN coated tools.

Further, when the apparent coefficient of friction (μ_{ap}), which is evaluated using Equation (2), is plotted against cutting speed, it is observed that the coated tools account to lower friction at the tool-chip interface (see Fig. 6). The lower friction coefficient values for the coated tools tend to reduce the standard deviation in machining forces while cutting with TiSiVN and TiSiN coated tools. Especially, TiSiVN coating's

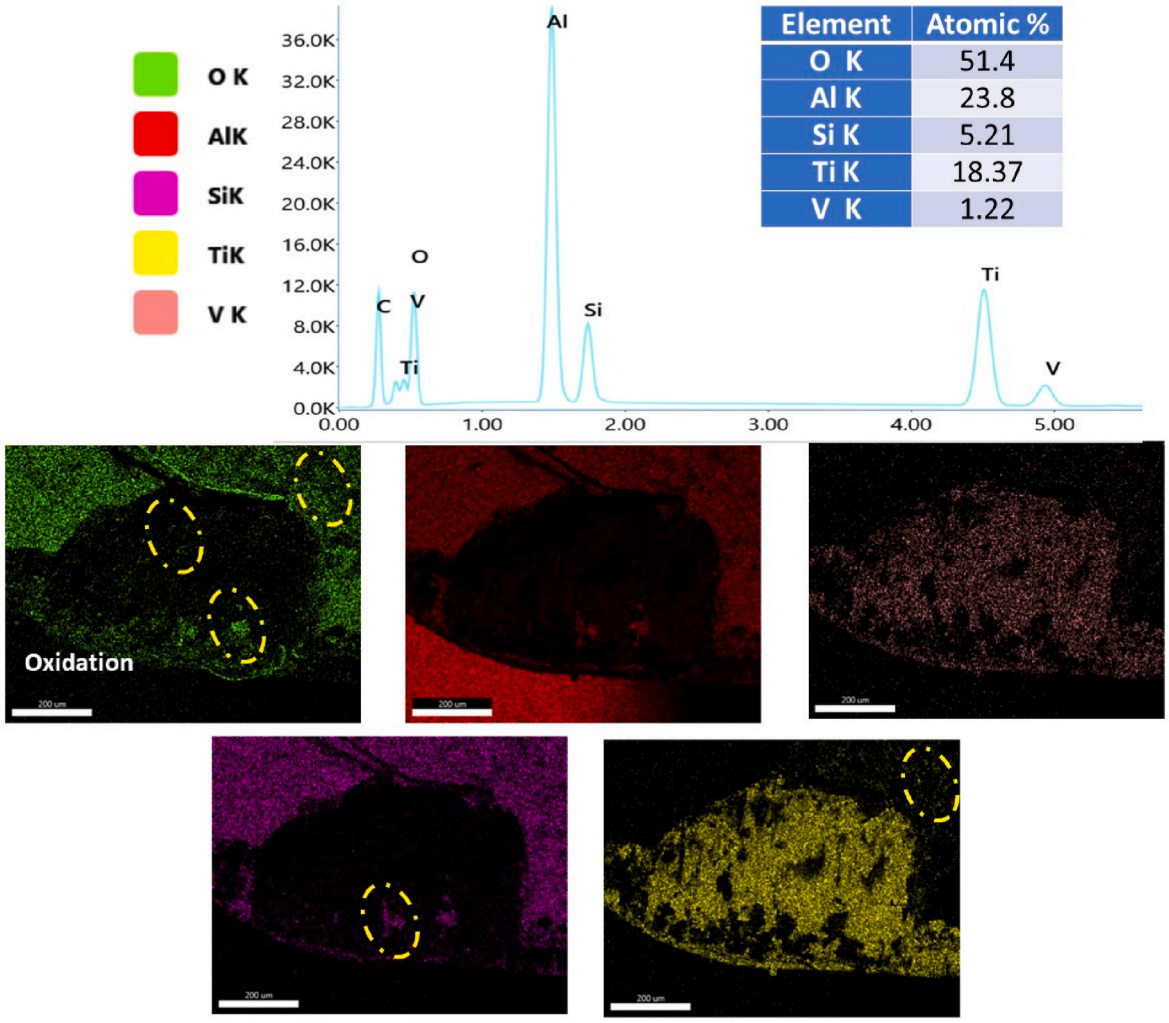

Fig. 11. EDS elemental mapping of region (c) from Fig. 11.

self-lubrication properties help in decreasing the friction to a much greater extent at the tool-chip interface, which is also apparent in the standard deviation of machining forces. Also, an increase in friction coefficient values can be seen with cutting speed. This increase can be due to increased tool wear with cutting speed [34]. However, the results of friction and forces are contradictory, requiring further investigation on tool wear and topography of cutting tools after machining.

3.3. Surface roughness

For both coated and uncoated tools, the measured average surface roughness (R_A) of the machined surface is plotted versus cutting speed in Fig. 7(a). Surface roughness has been found to rise as cutting speed increases, suggesting an increase in tool wear, which is also closely related to the standard deviation of machining forces and coefficient of friction. At a slower cutting speed of 50 m/min, coated and uncoated tools generate comparable surface roughness of the machined surface. Cutting using a tool coated with TiSiVN self-lubricating coating results in the superior surface quality of the machined surface with lower R_A values than TiSiN-coated tool when the cutting speed is increased to 75 m/min or higher. It is necessary to note that the standard deviation in surface roughness values is high basically due to significant deviation of machining forces owing to the adverse machining conditions adopted for the tests. Thus, in this scenario, only average values were considered to have a clear picture of the performance of cutting tools.

3.4. Cutting temperature

Fig. 7(b) shows the variation of cutting temperature with cutting speed for uncoated and coated cutting tools. The cutting temperatures increase with the increase in cutting speed which is a common phenomenon observed by many researchers [35]. The TiSiVN coating deposited on the whiskers-reinforced ceramic tool resulted in reduction of cutting temperatures owing to its self-lubricating properties and subsequent reduction of friction at the tool-chip interface. The rise in cutting temperature significantly increases tool wear rates due to increased material adhesion on the tool surface [28–30], and also due to increased diffusion wear at higher temperatures [5,36], there is severe deterioration of the cutting tool. Further, temperature also impacts crater formation on the rake face of the cutting tools during machining. Thus, the lower cutting temperatures for cutting tools with TiSiVN and TiSiN coatings should result in lower tool wear rates at higher cutting speeds. However, the different in temperatures for coated tools when compared to uncoated tool is not high which can again be attributed to the high standard deviation in machining forces causing significant changes during continuous temperature measurements.

3.5. Topography analysis

The crater wear on the cutting tool's rake face is substantially influenced by cutting speed. It has been noted that an increase in cutting

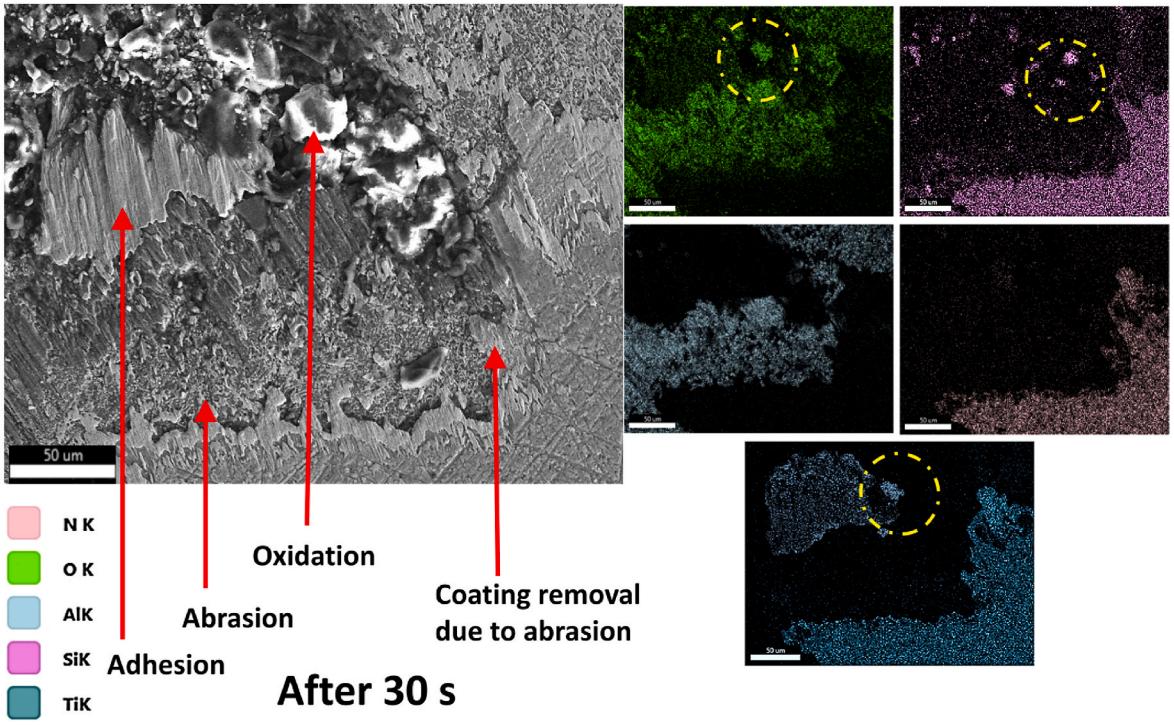

Fig. 12. SEM micrographs showing wear on the rake surface of TiSiN coated tool after 30 s of machining.

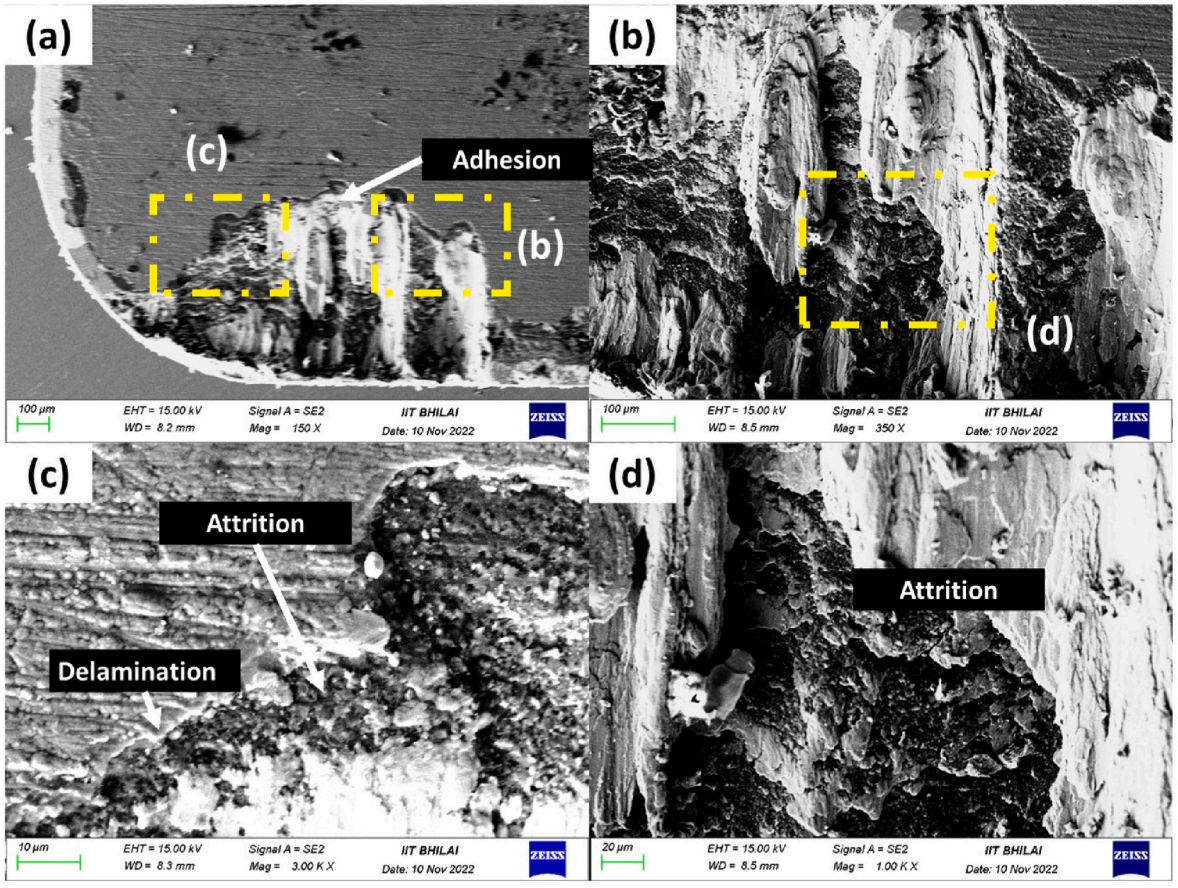

Fig. 13. SEM micrographs of the rake face of TiSiN coated Al_2O_3–SiC whiskers reinforced cutting tools after machining at 50 m/min cutting speed.

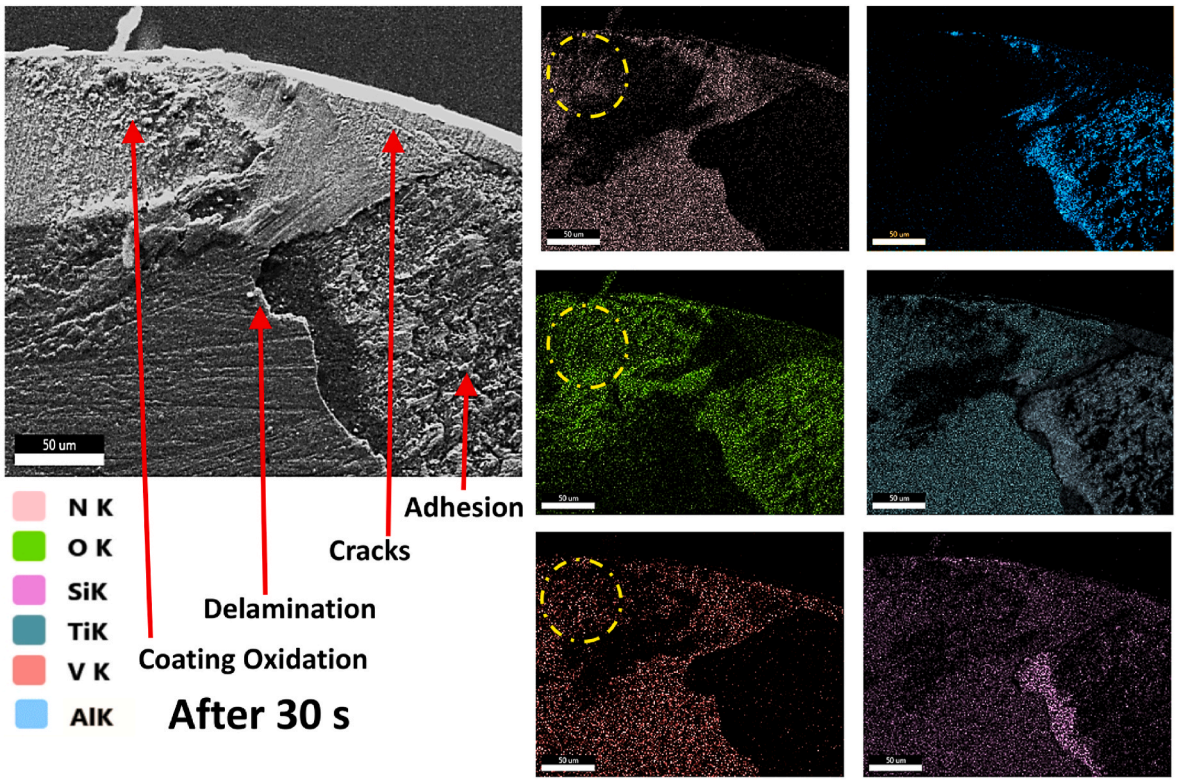

Fig. 14. SEM micrographs showing wear on the rake surface of TiSiVN coated tool after 30 s of machining.

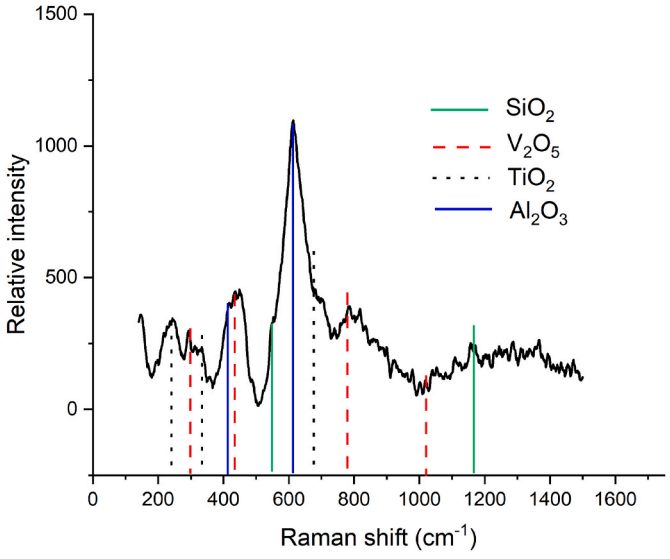

Fig. 15. Raman spectroscopy of the oxidation zone for TiSiVN coated tool.

speed results in a larger crater. However, detailed measurements of the crater volume (CV), crater area (CA), average crater depth (ACD), and nose depth decrement (NDD) are required for a better comprehension of the crater wear topography. Fig. 8 depicts an indicative measurement of these parameters made with Sensoview software, Version 1.6.0. In Fig. 9, the measured values of CV, CA, ACD, and NDD are plotted versus the cutting speed. As cutting speed increases, so do CV, ACD, and NDD.

However, CA grows with cutting speed up to 100 m/min, but at 125 m/min, there is a little drop that indicates a significant increase in NDD and ACD. The increased spread of CA results in higher CV values corresponding to TiSiN and TiSiVN coated tools. The higher CA is generated due to coating delamination caused by moving chips. However, the wear resistance of TiSiN due to its hardness [37] and self-lubricating properties of TiSiVN coatings may have overshadowed the effect of coating delamination at higher cutting speeds where the uncoated tool exhibited a severe increase in crater depth and nose depth decrement. The TiSiVN coating outperforms TiSiN coating under all circumstances. The coated tools showed excellent resistance to abrasive wear resulting in no drastic increase in the values of ACD and NDD with cutting speed up to 100 m/min, after which both the coated tools show a radical increase in these parameters indicating severe tool wear. On the contrary, the uncoated tool performs satisfactorily at 50 m/min after which increased cutting speed results in an exponential increase of ACD and NDD. The higher oxidation of TiSiVN coating at elevated cutting temperatures may have led to the formation of tribolayer (see Fig. 4) accounting to reduced friction. Thus, the TiSiVN coating helped the cutting tool to retain its nose depth more effectively at higher cutting speeds when compared to TiSiN coated and uncoated cutting tools. This caused the forces corresponding to TiSiN coated and uncoated tools to be higher at 125 m/min cutting speed when compared to TiSiVN coated tool basically due to decreased effective cutting depth for these tools.

3.6. Crater wear

In the previous sections, based on the tool topography after

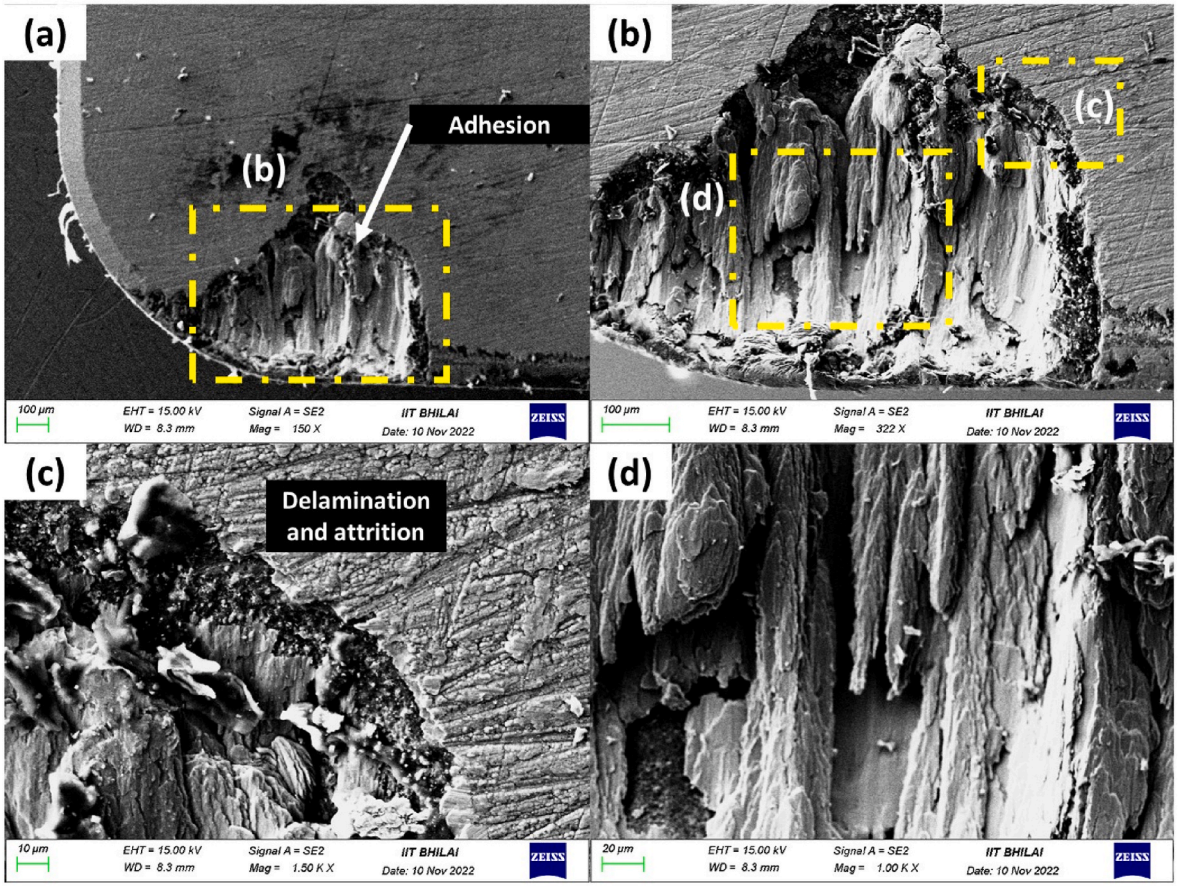

Fig. 16. SEM micrographs of the wear on the rake face of TiSiVN coated tool after machining at 50 m/min cutting speed.

machining, it was revealed that the coated tools accounted for lower crater depth values and nose depth decrement at all cutting speeds. In this section, a comprehensive discussion is made on the possible reasons for this superior performance of coated tools, especially with TiSiVN coating, compared to the uncoated cutting tool. Fig. 10 shows the SEM micrographs of the rake face of the uncoated Al_2O_3–SiC whiskers reinforced cutting after machining Ti6Al4V alloy at 50 m/min cutting speed. Fig. 10(b), (c), and 10(d) illustrate the magnified images of the marked regions outlined using yellow dashed lines. The SEM micrographs reveal that the wear on the rake face of the uncoated tool is characterized by adhesion, chip sticking, and seizure at the tool-chip interface leading to adhesion, attrition, and ploughing. Abrasive wear is not visible due to severe adhesion near the cutting edge.

Moreover, the crater is generally formed due to the chip movement over the rake face. However, due to high cutting temperatures as reported in Section 3.4. a considerable amount of adhesion was seen inside the crater, which is evident from the elemental mapping shown in Fig. 11. Further, from the magnified images, attrition due to adhesion and removal of material inside the crater, and ploughing due to movement of chips on the loosened surface formed after attrition can also be observed. Also, oxidation of tool and adhered workpiece material is evident from the EDS elemental mapping shown in Fig. 11.

Fig. 12 shows the wear on the rake surface of TiSiN coated tool after making a 30 s of machining. This stage has been analyzed to understand the initial wear mechanisms for the TiSiN coating. The wear on the coated tool is characterized by adhesion, abrasion, oxidation and coating removal due to abrasion. There are no signs of coating delamination and the coating removal is caused by only moving chips. However, oxidation of the coating material is evident from the EDS spectrum. Further, it is also evident that the coating retains its adhesion to the substrate.

The wear on the rake face of TiSiN coated tool (see Fig. 13) after completion of cutting pass is characterized by adhesion, seizure, attrition, and coating delamination. The attrition, in this case, is caused by coating delamination and the removal of adhered workpiece material inside the carter. Although the TiSiN coating resulted in reduced seizures at the tool-chip interface with no prominent chip sticking, the adhesion of workpiece material in the crater is quite prominent. Further, attrition inside the formed crater due to the removal of the adhered workpiece material is still visible for TiSiN coated tool. However, there are no signs of ploughing due to the movement of chips basically because of the high hardness offered by TiSiN coating.

Fig. 14 shows the SEM micrographs and elemental mapping on the rake face of the TiSiVN coated tool after 30 s. The wear on the TiSiVN coated tool is characterized by adhesion, oxidation, cracks on the coating surface, and coating delamination. The TiSiVN coating oxidizes rapidly as reflected by the TGA analysis, which causes delamination of coating on the surface due to reduced coating/substrate adhesion.

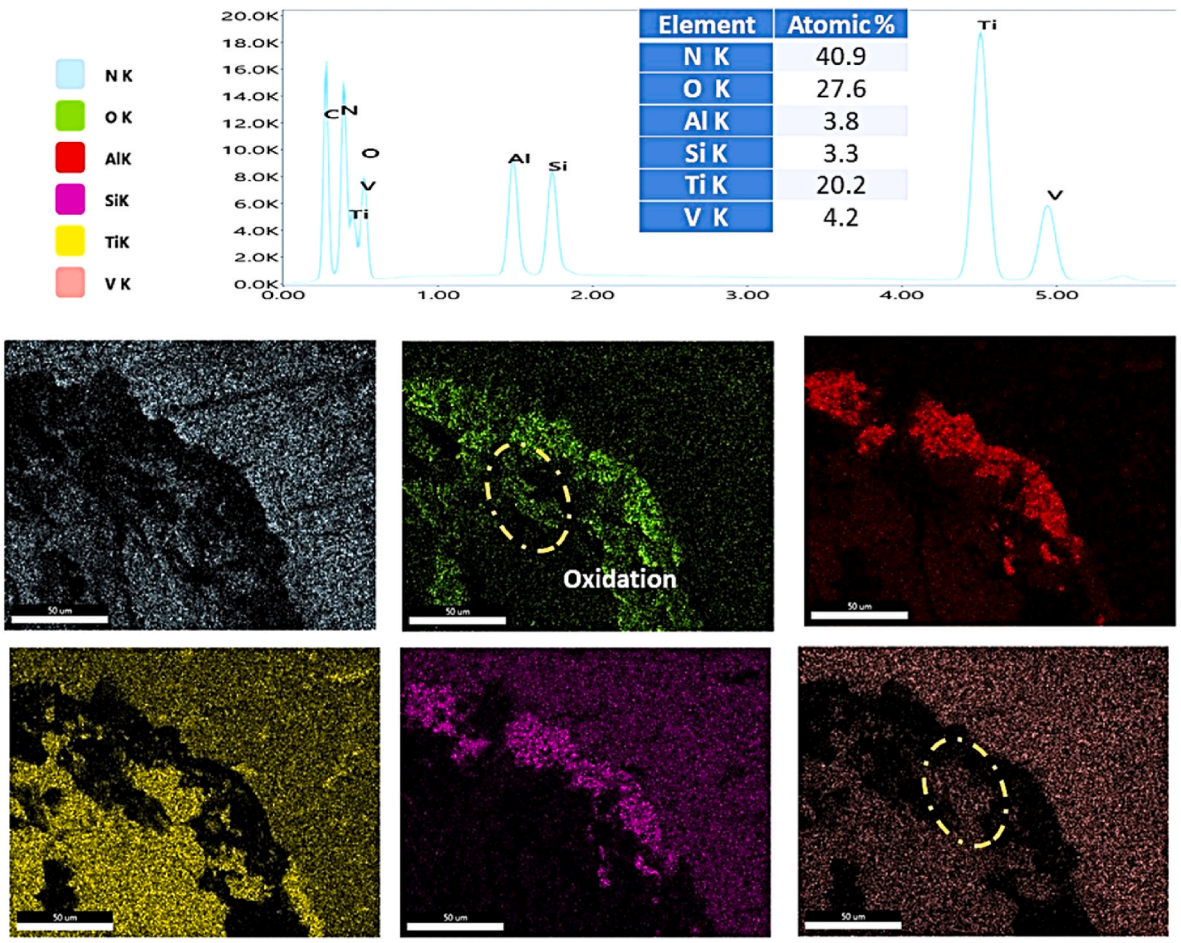

Fig. 17. EDS elemental mapping of region (c) from Fig. 16.

However, the oxidation of coating releases V_2O_5 oxides which act as lubricant in the cutting zone causing reduction of friction (see Fig. 6) during the machining operation. Raman spectrum (see Fig. 15) of the identified oxidation zone in Fig. 14 clearly shows the presence of oxides such as V_2O_5, TiO_2, SiO_2 and Al_2O_3 in the cutting zone which indicate oxidation of tool, workpiece, and coating material. The peaks have been identified from the previous published literature [20,38–41].

The wear on the rake face of TiSiVN coated tool (see Fig. 16) after completion of the cutting pass is characterized by adhesion, attrition, and coating delamination. The attrition, in this case, is caused by coating delamination. However, no signs of attrition and ploughing are visible inside the crater. Superior adhesion can be seen inside the formed crater, which is evident from the elemental mapping shown in Fig. 17. Also, the elemental mappings show signs of V oxidation, forming a self-lubricating phase helpful in reducing the friction that is also evident from the apparent friction coefficient results. Also, the coating effectively prevented seizure at the tool-chip interface, indicating its superior anti-adhesive properties. The presence of V in the workpiece material makes it difficult to determine the tribolayer formation between the tool and the moving chips during machining. However, when combined with oxidation results and measured temperature values, the coating inevitably oxidizes during machining.

3.7. Flank wear

After being machined at various cutting speeds using both coated and uncoated cutting tools, the flank surface observed using optical microscope is shown in Fig. 18. Further, Fig. 19 shows the depiction of the progression of flank wear relative to cutting speed. On the flank surface of all cutting tools, abrasion that results in groove creation may be noticed. The flank wear for all the cutting tools is comparatively equal at a cutting speed of 50 m/min. However, coated tools, particularly, those with TiSiVN coatings, outperform uncoated tools as the cutting speed is increased to 75 m/min and higher. The self-lubricating properties of the TiSiVN coating helped in reducing friction, which accounted for lower flank wear progression, with the uncoated, TiSiN-coated, and TiSiVN coated cutting tools failing at 75 m/min, 100 m/min, and 125 m/min cutting speeds, respectively.

To properly understand the variance in their machining performance, it is vital to understand the wear mechanism for every cutting tool used during machining. In this regard, Fig. 20 illustrates the micrographs obtained from the SEM of the flank surface following machining with an uncoated cutting tool at a cutting speed of 75 m/min. Abrasion, adhesion, chip sticking, and seizure are the main wear mechanisms on the flank surface of the uncoated cutting tool. A closer observation reveals adhesion and removal of adhered material, leading

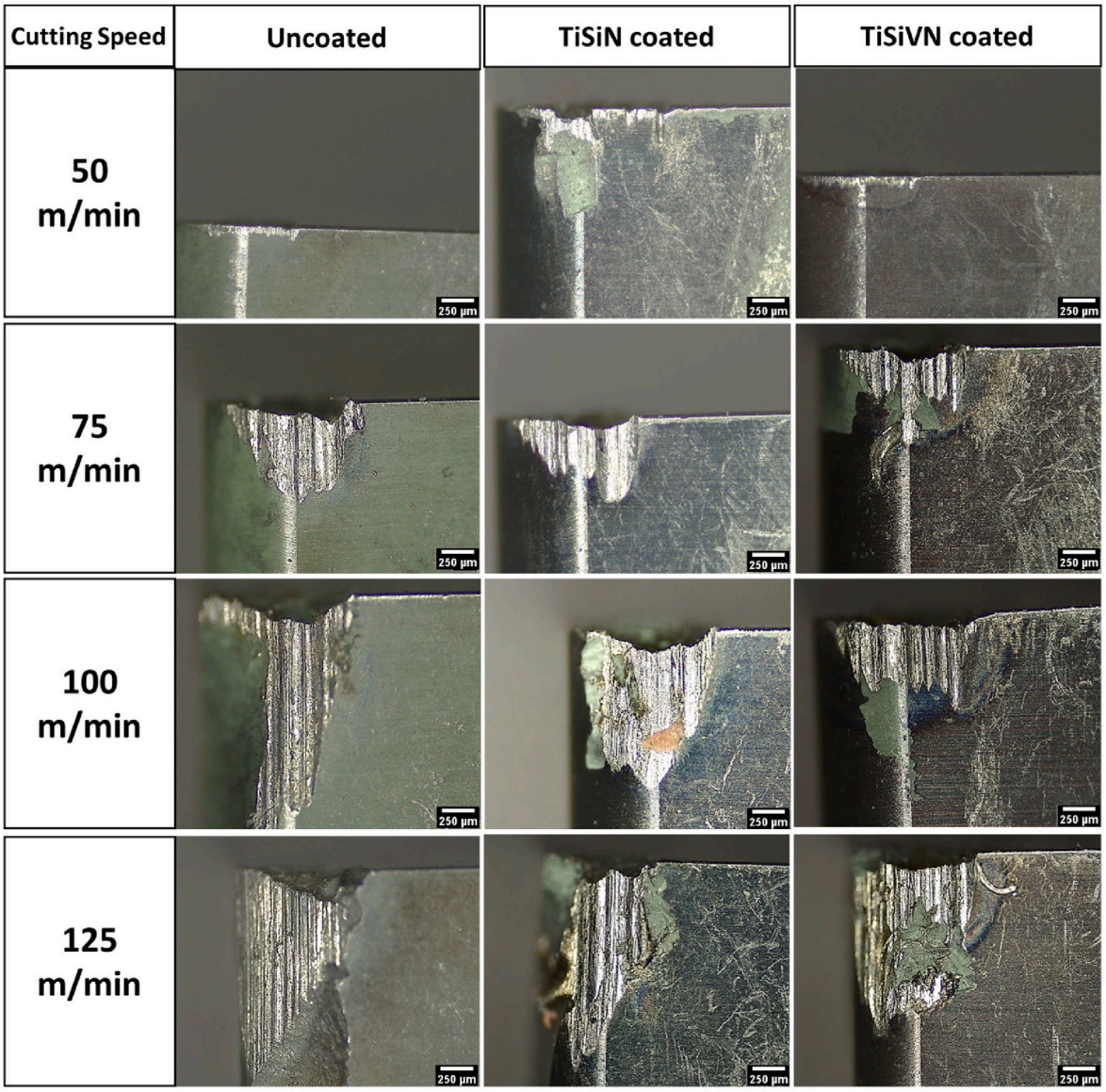

Fig. 18. Optical microscope images depicting wear on the flank surface after machining.

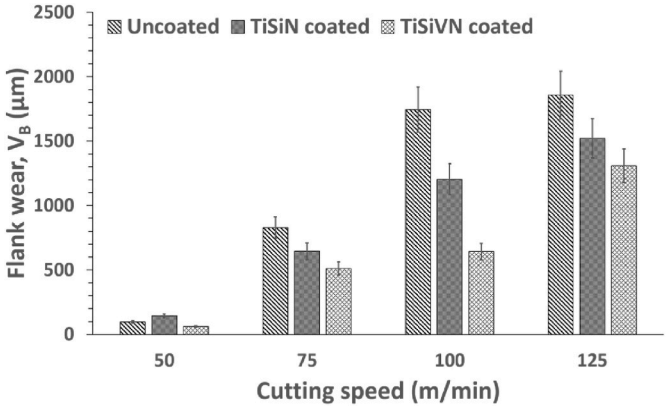

Fig. 19. Flank wear progression plotted against cutting speed.

to attrition within the grooved surface. Further, lamellar adhesion can be seen with trapped workpiece material elements within the tool material.

After machining at a cutting speed of 75 m/min, the TiSiN-coated cutting tool flank surface is depicted in SEM micrographs in Fig. 21. Abrasion, adhesion, seizure, chip sticking, and coating flaking are the characteristics of tool wear on the flank surface for tools coated with TiSiN. When compared to an uncoated tool, the coated surface had less seizure, demonstrating the TiSiN coating's improved anti-adhesive capabilities. Further, coating flanking can be seen in some places but is also not so prominent.

The wear on the flank surface of the TiSiVN-coated Al_2O_3–SiC cutting tool is seen in SEM micrographs in Fig. 22 following machining at a cutting speed of 75 m/min. The wear for TiSiVN coated tool is also characterized by adhesion, abrasion, seizure, coating delamination, and chip sticking. There are no signs of lamellar adhesion, but seizure on the coating surface is quite prominent. Further, the EDS elemental mapping

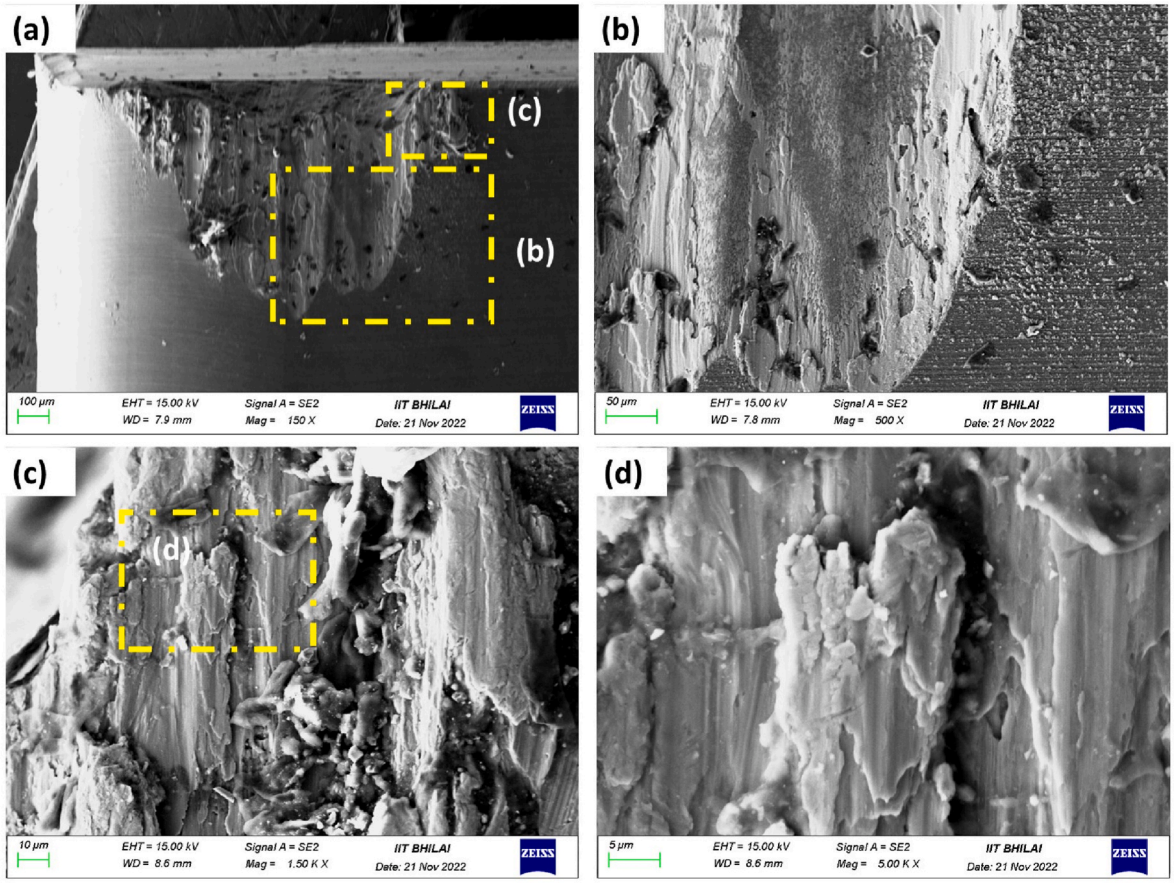

Fig. 20. SEM micrographs of the flank surface after machining with uncoated cutting tool at 75 m/min cutting speed.

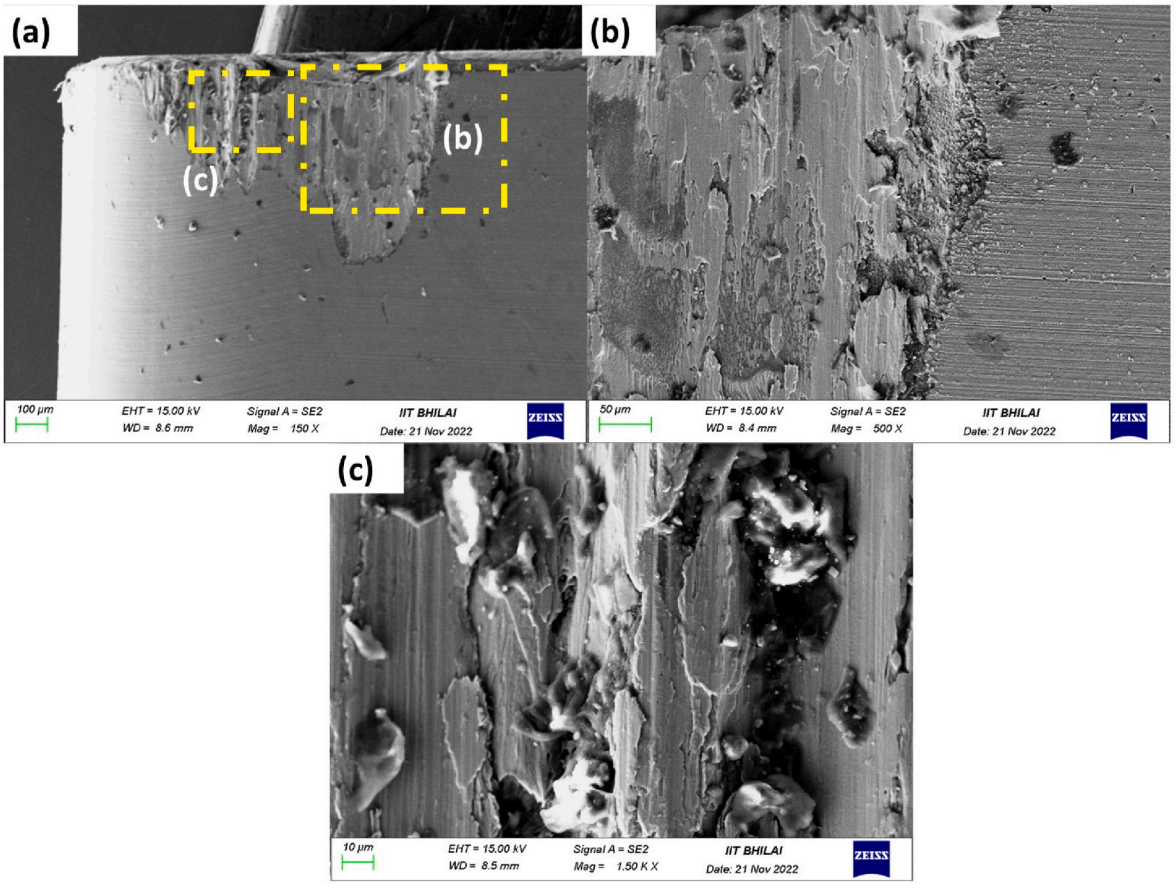

Fig. 21. SEM micrographs of the flank surface of TiSiN coated cutting tool after machining at 75 m/min cutting speed.

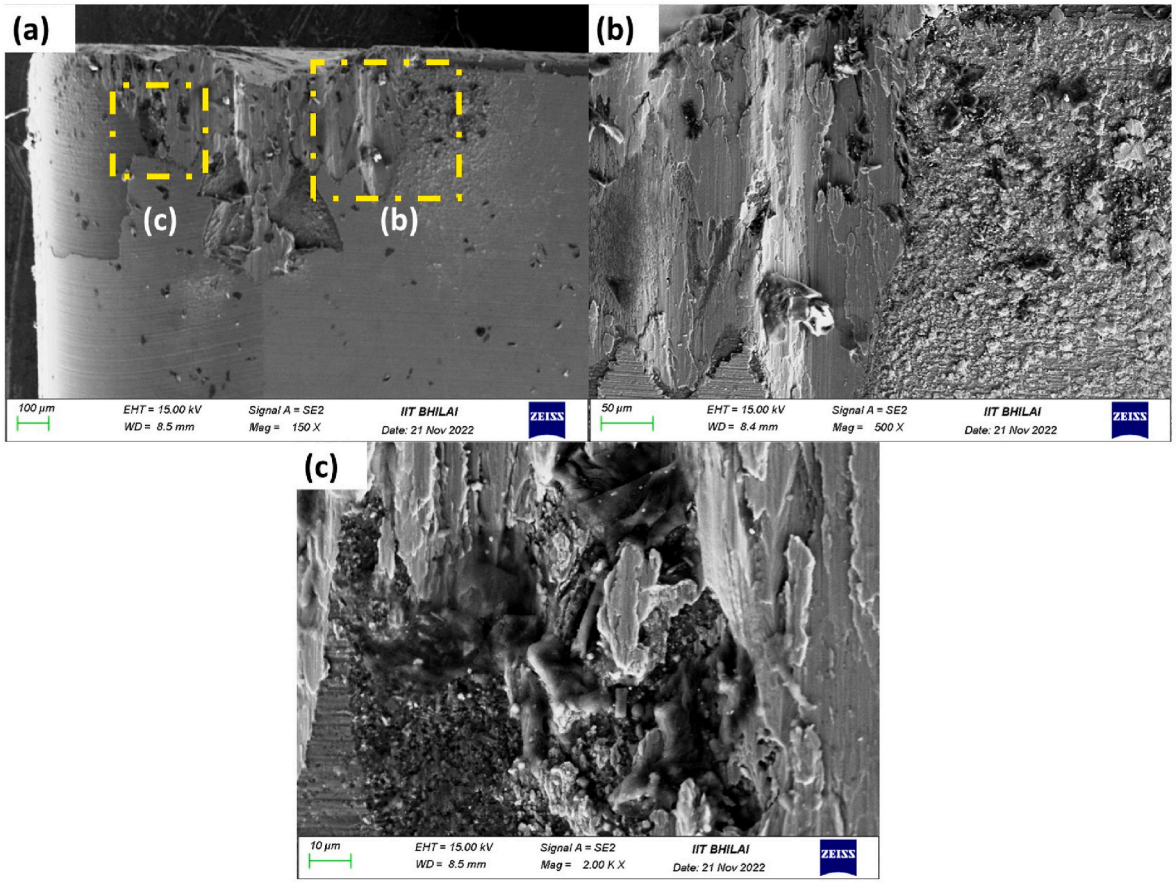

Fig. 22. SEM micrographs of wear on the flank surface of TiSiVN coated Al_2O_3–SiC cutting tool after machining at 75 m/min cutting speed.

shown in Fig. 23 provides evidence of tool and coating material oxidation. As discussed earlier, the oxidation of V present in TiSiVN coating results in the formation of lubricious phases that may help in reducing friction during machining. This reduction in friction would cause lower tool wear, as reported in Fig. 19.

4. Conclusions

In the present work, the TiSiVN coating's self-lubricating capabilities were investigated during dry turning of Ti6Al4V superalloy. From the obtained results, the following conclusions are drawn:

1. The TiSiVN coating accounts for a lower standard deviation in the machining forces compared to the uncoated and TiSiN-coated tools. The low friction lubricious phases generated during the machining process accounted to lower tool wear by reducing seizure at the tool-chip interface causing lower standard deviation in forces.
2. The crater volume, average crater depth, and nose depth decrement increases with an increase in cutting speed for both uncoated and coated cutting tools. However, crater area increases and then decreases due to severe reduction in the values of nose depth decrement and average crater depth.
3. The coated tools showed excellent resistance to abrasive wear resulting in no drastic increase in the values of average crater depth and nose depth decrement with cutting speed up to 100 m/min, after which both the coated tools show a radical increase in these parameters indicating severe tool wear.
4. The surface roughness and cutting temperatures increase with the increase in cutting speed for both uncoated and coated cutting tools. However, TiSiVN coated tool accounted to lower surface roughness and cutting temperatures at higher cutting speeds.
5. The elemental mapping and Raman spectrum of the TiSiVN coated tool after machining showed signs of V oxidation, which would form a self-lubricating phase, possibly V_2O_5, as observed during oxidation tests that would help to reduce friction which is also evident from the apparent friction coefficient results. Also, the generation of lubricious phases during machining helped the coating to reduce the seizure at the tool-chip interface effectively.

From the above conclusions, it is apparent that the TiSiVN coating reduced friction to some extent due to the generation of lubricious phases but delamination due to oxidation was the major issue that needs to be addressed. The coatings help to improve the machining performance over uncoated tools. However, TiSiVN coating offers a marginal improvement over TiSiN coating at lower cutting speeds, but the improvement is noticeable at higher speeds.

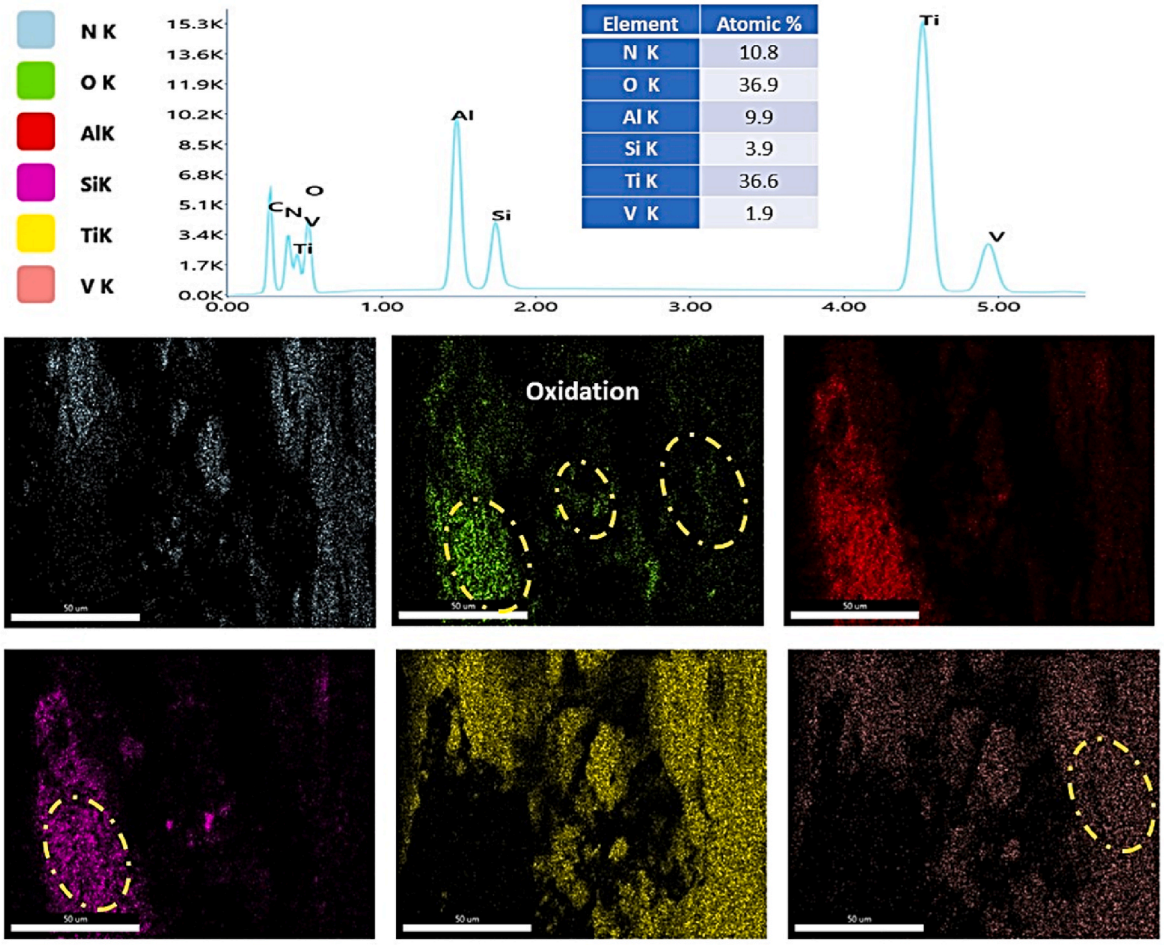

Fig. 23. EDS elemental mapping of region (c) from Fig. 22.

Declaration of competing interest

The authors declare that they have no known competing financial interests or personal relationships that could have appeared to influence the work reported in this paper.

Data availability

Data will be made available on request.

Acknowledgment

The work is supported by Maria Zambrano grants. Thanks are addressed to project PDC2021-121792-I00 (HCR Taylor) funded by MCIN/AEI/10.13039/501100011033 and by European Union Next Generation EU/PRTR and Project ITENEO (DPI2016-74845-R) MCIN/AEI/10.13039/501100011033. The authors also thank SGIker (UPV/EHU/ERDF, EU) for technical and human support. This research is also sponsored by FEDER Funds through Portugal 2020 (PT2020), by the Competitiveness and Internationalization Operational Program (COMPETE 2020), and national funds through the Portuguese Foundation for Science and Technology (FCT) under the projects: MCTool21-ref:" POCI-01-0247-FEDER-045940", UIDB/00285/2020 and LA/P/0112/2020.

References

[1] M. Strano, P. Albertelli, E. Chiappini, S. Tirelli, Wear behaviour of PVD coated and cryogenically treated tools for Ti-6Al-4V turning, Int. J. Material Form. 8 (2015) 601–611, https://doi.org/10.1007/s12289-014-1215-6.

[2] S. Koseki, K. Inoue, K. Sekiya, S. Morito, T. Ohba, H. Usuki, Wear mechanisms of PVD-coated cutting tools during continuous turning of Ti-6Al-4V alloy, Precis. Eng. 47 (2017) 434–444, https://doi.org/10.1016/j.precisioneng.2016.09.018.

[3] A. Hosseini, H.A. Kishawy, Machining of titanium alloys. https://doi.org/10.1007/978-3-662-43902-9, 2014.

[4] A. Daymi, M. Boujelbene, S. Ben Salem, B. Hadj Sassi, S. Torbaty, B.H. Sassi, Effect of the cutting speed on the chip morphology and the cutting forces, Manuf.Process. Eng. Mater. 78 (1) (2009) 77–83.

[5] A. Biksa, K. Yamamoto, G. Dosbaeva, S.C. Veldhuis, G.S. Fox-Rabinovich, A. Elfizy, T. Wagg, L.S. Shuster, Wear behavior of adaptive nano-multilayered AlTiN/MexN PVD coatings during machining of aerospace alloys, Tribol. Int. 43 (2010) 1491–1499, https://doi.org/10.1016/j.triboint.2010.02.008.

[6] T.C.S. Vandevelde, K. Vandierendonck, M. Van Stappen, W. Du Mong, P. Perremans, Cutting applications of DLC, hard carbon and diamond films, Surf. Coat.Technol. 113 (1999) 80–85, https://doi.org/10.1016/S0257-8972(98)00831-7.

[7] S.B. Hosseini, T. Beno, U. Klement, J. Kaminski, K. Ryttberg, Cutting temperatures during hard turning - measurements and effects on white layer formation in AISI 52100, J. Mater. Process. Technol. 214 (2014) 1293–1300, https://doi.org/10.1016/j.jmatprotec.2014.01.016.

[8] X. Sui, G. Li, X. Qin, H. Yu, X. Zhou, K. Wang, Q. Wang, Relationship of microstructure, mechanical properties and titanium cutting performance of TiAlN/TiAlSiN composite coated tool, Ceram. Int. 42 (2016) 7524–7532, https://doi.org/10.1016/j.ceramint.2016.01.159.

[9] M.A. El Hakim, M.D. Abad, M.M. Abdelhameed, M.A. Shalaby, S.C. Veldhuis, Wear behavior of some cutting tool materials in hard turning of HSS, Tribol. Int. 44 (2011) 1174–1181, https://doi.org/10.1016/j.triboint.2011.05.018.

[10] H. Çalişkan, C. Kurbanoğlu, P. Panjan, M. Čekada, D. Kramar, Wear behavior and cutting performance of nanostructured hard coatings on cemented carbide cutting tools in hard milling, Tribol. Int. 62 (2013) 215–222, https://doi.org/10.1016/j.triboint.2013.02.035.

[11] T. Özel, M. Sima, A.K. Srivastava, B. Kaftanoglu, Investigations on the effects of multi-layered coated inserts in machining Ti-6Al-4V alloy with experiments and finite element simulations, CIRP Ann. - Manuf. Technol. 59 (2010) 77–82, https://doi.org/10.1016/j.cirp.2010.03.055.

[12] W. Kalss, A. Reiter, V. Derflinger, C. Gey, J.L. Endrino, Modern coatings in high performance cutting applications, Int. J. Refract. Met. Hard Mater. 24 (2006) 399–404, https://doi.org/10.1016/j.ijrmhm.2005.11.005.

[13] A. Mkaddem, A. Ben Soussia, M. El Mansori, Wear resistance of CVD and PVD multilayer coatings when dry cutting fiber reinforced polymers (FRP), Wear 302 (2013) 946–954, https://doi.org/10.1016/j.wear.2013.03.017.
[14] C.S. Kumar, S.K. Patel, Surface & Coatings Technology Experimental and numerical investigations on the effect of varying AlTiN coating thickness on hard machining performance of Al 2 O 3 -TiCN mixed ceramic inserts, SCT 309 (2017) 266–281, https://doi.org/10.1016/j.surfcoat.2016.11.080.
[15] C. Sateesh Kumar, S. Kumar Patel, Hard machining performance of PVD AlCrN coated Al2O3/TiCN ceramic inserts as a function of thin film thickness, Ceram. Int. 43 (2017) 13314–13329, https://doi.org/10.1016/j.ceramint.2017.07.030.
[16] D. Cavaleiro, D. Figueiredo, C.W. Moura, A. Cavaleiro, S. Carvalho, Machining performance of TiSiN (Ag) coated tools during dry turning of TiAl6V4 aerospace alloy, Ceram. Int. 47 (2021) 11799–11806, https://doi.org/10.1016/j.ceramint.2021.01.021.
[17] A. Al-rjoub, T. Bin, A. Cavaleiro, F. Fernandes, The influence of V addition on the structure , mechanical properties , and oxidation behaviour of TiAlSiN coatings deposited by DC magnetron sputtering, J. Mater. Res. Technol. 20 (2022) 2444–2453, https://doi.org/10.1016/j.jmrt.2022.08.009.
[18] R. Franz, C. Mitterer, Vanadium containing self-adaptive low-friction hard coatings for high-temperature applications: a review, Surf. Coat.Technol. 228 (2013) 1–13, https://doi.org/10.1016/j.surfcoat.2013.04.034.
[19] C. Sateesh, H. Majumder, A. Khan, S. Kumar, Applicability of DLC and WC/C low friction coatings on Al 2 O 3/TiCN mixed ceramic cutting tools for dry machining of hardened 52100 steel, Ceram. Int. (2020) 0–1, https://doi.org/10.1016/j.ceramint.2020.01.225.
[20] F. Fernandes, J. Morgiel, T. Polcar, A. Cavaleiro, Oxidation and diffusion processes during annealing of TiSi(V)N films, Surf. Coat.Technol. 275 (2015) 120–126, https://doi.org/10.1016/j.surfcoat.2015.05.031.
[21] Y.M. Ko, W.T. Kwon, Y.W. Kim, Development of Al2O3-SiC composite tool for machining application, Ceram. Int. 30 (2004) 2081–2086, https://doi.org/10.1016/j.ceramint.2003.11.011.
[22] T. Brzezinka, J. Rao, J. Paiva, J. Kohlscheen, G. Fox-Rabinovich, S. Veldhuis, J. Endrino, DLC and DLC-WS2 coatings for machining of aluminium alloys, Coatings 9 (2019) 192, https://doi.org/10.3390/coatings9030192.
[23] W. Yang, J. Xiong, Z. Guo, H. Du, T. Yang, J. Tang, B. Wen, Structure and properties of PVD TiAlN and TiAlN/CrAlN coated Ti(C, N)-based cermets, Ceram. Int. 43 (2016) 1911–1915, https://doi.org/10.1016/j.ceramint.2016.10.151.
[24] C.S. Kumar, P. Zeman, T. Polcar, A 2D finite element approach for predicting the machining performance of nanolayered TiAlCrN coating on WC-Co cutting tool during dry turning of AISI 1045 steel, Ceram. Int. 46 (2020) 25073–25088, https://doi.org/10.1016/j.ceramint.2020.06.294.
[25] M.J. Bermingham, W.M. Sim, D. Kent, S. Gardiner, M.S. Dargusch, Tool life and wear mechanisms in laser assisted milling Ti-6Al-4V, Wear 322–323 (2015) 151–163, https://doi.org/10.1016/j.wear.2014.11.001.
[26] S. Rodríguez-Barrero, J. Fernández-Larrinoa, I. Azkona, L.N.L. de Lacalle, R. Polvorosa, Enhanced performance of nanostructured coatings for drilling by droplet elimination, Mater. Manuf. Process. 31 (2016) 593–602, https://doi.org/10.1080/10426914.2014.973582.
[27] A.I. Fernández-Abia, J. Barreiro, L.N. López de Lacalle, S. Martínez-Pellitero, Behavior of austenitic stainless steels at high speed turning using specific force coefficients, Int. J. Adv. Manuf. Technol. 62 (2012) 505–515, https://doi.org/10.1007/s00170-011-3846-9.
[28] A.I. Fernández-Abia, J. Barreiro, L.N.L. de Lacalle, S. Martínez, Effect of very high cutting speeds on shearing, cutting forces and roughness in dry turning of austenitic stainless steels, Int. J. Adv. Manuf. Technol. 57 (2011) 61–71, https://doi.org/10.1007/s00170-011-3267-9.
[29] J. Patscheider, T. Zehnder, M. Diserens, Structure-performance relations in nanocomposite coatings, Surf. Coat.Technol. 146–147 (2001) 201–208, https://doi.org/10.1016/S0257-8972(01)01389-5.
[30] F. Fernandes, S. Calderon V, P.J. Ferreira, A. Cavaleiro, J.C. Oliveira, Low peak power deposition regime in HiPIMS: deposition of hard and dense nanocomposite Ti-Si-N films by DOMS without the need of energetic bombardment, Surf. Coat. Technol. 397 (2020), 125996, https://doi.org/10.1016/j.surfcoat.2020.125996.
[31] F. Fernandes, A. Loureiro, T. Polcar, A. Cavaleiro, The effect of increasing V content on the structure, mechanical properties and oxidation resistance of Ti–Si–V–N films deposited by DC reactive magnetron sputtering, Appl. Surf. Sci. 289 (2014) 114–123, https://doi.org/10.1016/j.apsusc.2013.10.117.
[32] Y. Moritz, C. Saringer, M. Tkadletz, A. Stark, N. Schell, I. Letofsky-Papst, C. Czettl, M. Pohler, N. Schalk, Oxidation behavior of arc evaporated TiSiN coatings investigated by in-situ synchrotron X-ray diffraction and HR-STEM, Surf. Coat. Technol. 404 (2020), 126632, https://doi.org/10.1016/j.surfcoat.2020.126632.
[33] F. Fernandes, J.C. Oliveira, A. Cavaleiro, Self-lubricating TiSi(V)N thin films deposited by deep oscillation magnetron sputtering (DOMS), Surf. Coat.Technol. 308 (2016) 256–263, https://doi.org/10.1016/j.surfcoat.2016.07.039.
[34] D. Ulutan, T. Özel, Determination of tool friction in presence of flank wear and stress distribution based validation using finite element simulations in machining of titanium and nickel based alloys, J. Mater. Process. Technol. 213 (2013) 2217–2237, https://doi.org/10.1016/j.jmatprotec.2013.05.019.
[35] C.S. Kumar, S.K. Patel, Performance analysis and comparative assessment of nano-composite TiAlSiN/TiSiN/TiAlN coating in hard turning of AISI 52100 steel, Surf. Coat.Technol. 335 (2018) 265–279, https://doi.org/10.1016/j.surfcoat.2017.12.048.
[36] H.O. Gekonde, S. V Subramanian, Tribology of tool – chip interface and tool wear mechanisms, Surf. Coat.Technol. 149 (2002) 151–160, https://doi.org/10.1016/S0257-8972(01)01488-8.
[37] R. M'Saoubi, M.P. Johansson, J.M. Andersson, Wear mechanisms of PVD-coated PCBN cutting tools, Wear 302 (2013) 1219–1229, https://doi.org/10.1016/j.wear.2013.01.074.
[38] W.F. Zhang, Y.L. He, M.S. Zhang, Z. Yin, Q. Chen, Raman scattering study on anatase TiO2 nanocrystals, J. Phys. D Appl. Phys. 33 (2000) 912–916, https://doi.org/10.1088/0022-3727/33/8/305.
[39] Q. Su, C.K. Huang, Y. Wang, Y.C. Fan, B.A. Lu, W. Lan, Y.Y. Wang, X.Q. Liu, Formation of vanadium oxides with various morphologies by chemical vapor deposition, J. Alloys Compd. 475 (2009) 518–523, https://doi.org/10.1016/j.jallcom.2008.07.078.
[40] M. Ivanda, R. Clasen, M. Hornfeck, W. Kiefer, Raman spectroscopy on SiO2 glasses sintered from nanosized particles, J. Non-Cryst. Solids 322 (2003) 46–52, https://doi.org/10.1016/S0022-3093(03)00172-8.
[41] F. Gyakwaa, T. Alatarvas, Q. Shu, M. Aula, T. Fabritius, Characterization of Synthetic Non-metallic Inclusions, 2021.